CHAPTER 6

THE STRUCTURES OF CYCLIC VINYLOGOUS AMIDES

6.1. Background

6.1.1. *E*, *Z*- isomerism in enaminones

It is well known that, owing to restricted rotation about the C=C bond, vinylogous amides (or "enaminones") can adopt various conformations [165]. Usually, tertiary enaminones **317** prefer to adopt the *E*-configuration about the C=C bond, whereas primary or secondary vinylogous amides **317** adopt the *Z*-configuration about this bond.

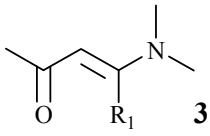

317

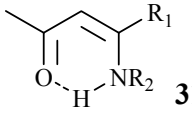

318

(R_1, R_2 = H, or an alkyl group)

Owing to steric hindrance in **317**, the *E*-configuration is preferred, whereas the stabilizing effect of intramolecular hydrogen bonding in **318** favours the *Z*-configuration. Evidence for this interesting phenomenon comes from the characterization data obtained of enaminones over many years. For example, ^{1}H NMR spectroscopy usually conveys a deshielding effect on the hydrogen(s) bonded to the first or α- carbon in the R_1 substituent (if R_1 = an alkyl group) in **317**, owing to the close proximity of these hydrogens to the highly electronegative carbonyl oxygen in **317**. On the other hand, the N*H* hydrogen is significantly deshielded in **318** as a result of the hydrogen bonding. X-ray crystallography of various enaminone-containing compounds has further confirmed this geometric isomerism.

Our successful model synthetic studies discussed in Chapter 3 made possible the easy access to a variety of cyclic vinylogous amides inspired by the structure of febrifugine (**1**). Most of the model vinylogous amides obtained in Chapter 3 are crystalline compounds, which were found to be very suitable for single crystal growth. The quinazolinone moiety in these compounds is thought to contribute significantly to

their highly crystalline nature, owing to the planar nature of this relatively polar heteroaromatic residue. It was decided to use single crystal X-ray diffraction studies, together with the NMR characterization data for the model enaminones, in order to elaborate further on the existing knowledge regarding geometric isomerism in enaminones.

6.1.2. The influence of ring size on the structures of cyclic amides

To demonstrate the way in which ring size might influence conformation in a series of compounds, we will discuss here the effect of ring size on the structures of thiolactams. During 1967-1969, Hallam and Jones [166] published an interesting series of papers on the structures of lactams, thiolactams and selenolactams. It was discovered, using infrared spectroscopy, that these cyclic amides can exist either in the *cis*- or in the *trans*- conformation depending on the ring size (Figure 29). The terms *cis* and *trans* describe the relative orientation of the carbonyl and N-H units.

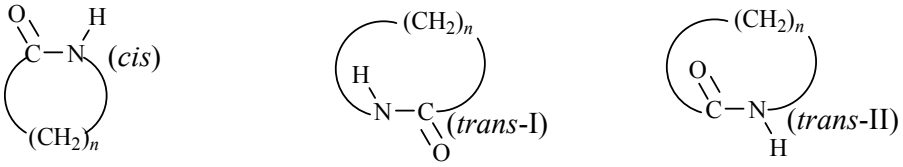

Figure 29.

It is obvious that the amide functional group would be constrained in smaller rings to adopt the *cis*-conformation. Neither the carbonyl group (*trans*-II, Figure 29) nor the NH (*trans*-I) can be rotated inwards into the ring for steric reasons. The question is at what point, as the ring size increases, is this constraint no longer spatially enforced?

The *cis*→*trans* transition could be easily determined by studying the N-H infrared absorption bands. A distinguishable difference in N-H stretching frequencies between the *cis*- and *trans*-conformers has been theoretically described by Moritz [166] to be as result of the "field-effect" of the carbonyl group. This effect causes a distinct increase in the N-H stretching frequency for the *cis*→*trans* transition. Furthermore, this effect decreases depending on the type of carbonyl bond in the following order: C=O > C=S

> C=Se. The *v*(NH) frequency ranges (in CCl_4 solution) for the *cis*- and *trans*-isomers are therefore well separated in the lactams (3430-3397 cm^{-1} for *cis*; 3470-3452 cm^{-1} for *trans*), meet in the thiolactams (3400-3360 cm^{-1} for *cis*; 3430-3400 cm^{-1} for *trans*), and overlap in the selenolactams (3387.5-3356 cm^{-1} for *cis*; 3395-3375.5 cm^{-1} for *trans*). It can be seen that the N-H stretching frequencies generally decrease in the following order: C=O > C=S > C=Se. This happens because there is an increased contribution from the more polar resonance form (**319**), and a decreased contribution from the neutral form (**320**), through this series.

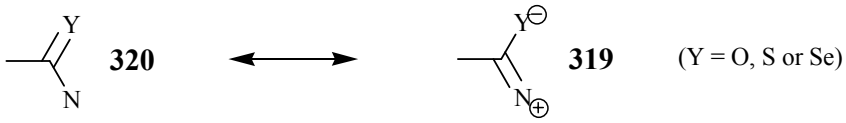

The increased electron-withdrawal from the nitrogen through the series, O < S < Se, is responsible for the above-mentioned effect. An increased contribution from **319** causes a weakening of the N-H bond by reducing the electron density in this bond. This leads to a lowering of the N-H stretching frequency. This is also the reason why thioamides, as opposed to amides, are reactive towards alkyl halides in the Eschenmoser reaction. Selenolactams would therefore be expected to be even more reactive than thioamides in the Eschenmoser reaction.

The results in the Hallam and Jones papers [166] are intriguing. In all three groups of cyclic amides studied (i.e. the oxylactams, the thiolactams and the selenolactams), the *cis*→*trans* transition occurs gradually at the two 8→10-membered ring transitions, in each case. Hallam and Jones found that, in fact, six different conformers in total are detectable by IR in CCl_4 solution; two *trans* forms (*trans*-I and II, Figure 29), two *cis* forms (i.e. two different "buckled" structures of the ring), and two "skew" forms (corresponding to intermediate forms, between *cis* and *trans*). Their results for the thiolactams are summarized in Table 24. It can be seen that the five-, six- and seven-membered (*n* = 3, 4 and 5, refer to Figure 29 on the previous page) thiolactams adopt exclusively a single, simple *cis*-conformation. The eight-membered (*n* = 6) thiolactam adopts two "buckled" *cis*-conformers. The nine-membered (*n* = 7) thiolactam also adopts these two *cis*-conformers, in addition to the two "skew" conformers. The 10-membered- (*n* = 8, Figure 29) and larger rings exclusively adopt the two *trans*-conformers.

n	Band	*trans*-I	*trans*-II	skew-I	skew-II	*cis* I		*cis* II
3							3428.5	
4							3385	
5							3399.5	
6						3384.5		3381
7				3418	3403	3382.5		3368
8	ca. 3430 (shld)	3422.5	Shld					3360
9		3421	3408					
10		3420	3406					
11		3418.5	3401.5					
14		3416	3403.5					

Table 24: Representation of Hallam and Jones' [166] IR (N-H bands) results with thiolactams (in CCl_4 solution). The frequencies given are in cm^{-1}. See the accompanying Figure 29 before. (shld = shoulder)

During our model studies, we synthesized the 13-membered thiolactam, azacyclotridecane-2-thione **142**. Two broad N-H bands (a strong, broad absorption at 3203 cm^{-1} and a medium, broad absorption at 3053 cm^{-1}) were indeed observed in the solid-state IR spectrum of **142**. These bands were at the same frequencies as those observed by Hallam and Jones for **142** *in the solid-state*. The large difference in N-H frequencies between the dissolved (diluted) cyclic amide (as given before) and the solid-state compound is a result of intermolecular association, e.g. by hydrogen bonding, in the solid-state. Such aggregation weakens the N-H bond, which leads to a lowering of the absorption frequencies. The band observed at 3203 cm^{-1} in the spectrum of the pure compound is still an indication that **142** adopts exclusively the *trans* configuration. The accompanying band at *ca*. 3050 cm^{-1} was also observed by Hallam and Jones. They mentioned that this band is an overtone of the 1150 cm^{-1} band in Fermi resonance with the corresponding fundamental *v*(NH) band. A similar absorption band was observed in the *cis* compounds, but the main NH band was at a considerably lower frequency (*ca*. 3170 cm^{-1}) in the solid-state *cis* cyclic amides.

As no similar study regarding the influence of ring size on cyclic vinylogous amide conformation has ever been conducted, we decided to embark on such a study during this project. The aim was to obtain and compare the X-ray diffraction data, together with the NMR data, of cyclic vinylogous amides of varying ring size. The crystalline model compounds obtained in Chapter 3 were used for this purpose.

6.1.3. Brown's hypothesis

In 1954, Herbert Brown and co-workers [167] published a theoretical paper on the relative stabilities of double bonds endo- and exocyclic to five- and six-membered rings. An extensive survey was conducted on chemical reactions and chemical equilibria involving double bonds in five- and six-membered rings. The results led Brown to make the following generalized statement, which we will refer to as "Brown's hypothesis": *reactions will proceed in such a manner as to favor the formation or retention of an exo double bond in the 5-ring and to avoid the formation or retention of the exo double bond in the 6-ring systems.* A few illustrations, in support of this hypothesis, are as follows:

A. The solvolysis of tertiary halides in aqueous ethanol, which results in a change from *tetrahedral* to *trigonal* geometry (i.e. similar to going from the saturated to the unsaturated state) of a ring carbon, occurs much more rapidly in the 5-membered ring than in the six-membered ring:

$$RCl + H_2O \rightleftharpoons R^+ + Cl^- \qquad k^{25°C}\ (hour^{-1})$$

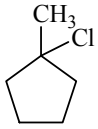

$k^{25°C} = 1.32$

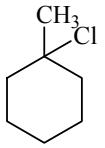

$k^{25°C} = 0.0106$

B. Olefin formation, by the dehydration of tertiary alcohols, usually occurs according to Saytzeff's rule, i.e. elimination gives the more highly substituted olefin [see (i) and (iv) below]. This is not observed for the corresponding cyclohexane tertiary alcohol [see (ii) and (iii) below], whereas the cyclopentane alcohol in (iv) does comply with this rule.

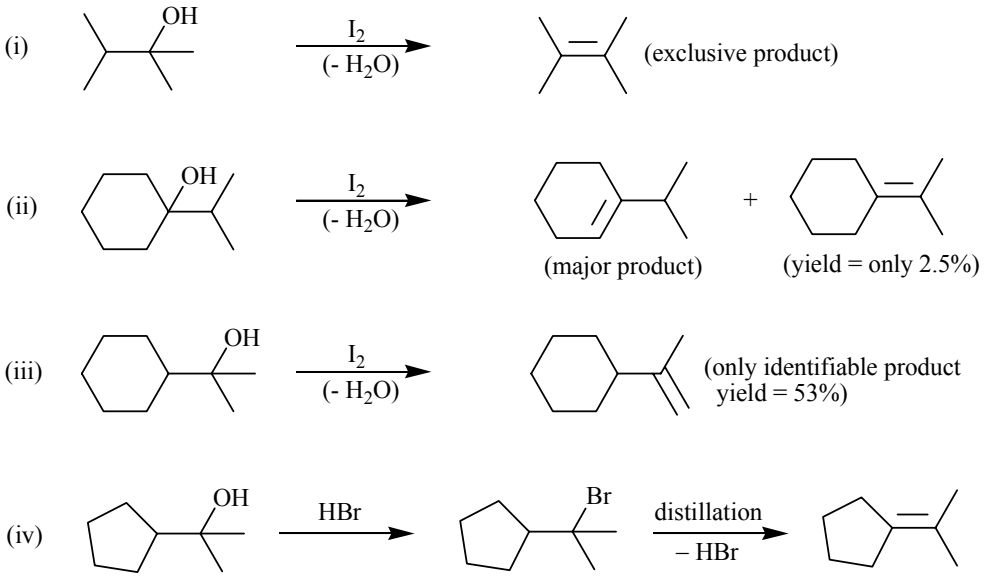

C. Brown also used the well-known structures of sugar acids and sugar aldehydes in support of his hypothesis, i.e. any given sugar lactone with an exocyclic double bond (C=O) prefers the 5-membered ring [see (ii) below], whereas the corresponding hemiacetal [without an exocyclic double bond, see (i) below] prefers the 6-membered ring:

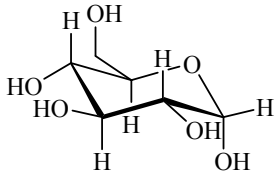

(i) α-D-glucose

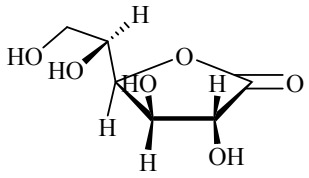

(ii) α-D-gluconolactone

Brown's hypothesis was subsequently questioned in 1957 by Fleck [168] who realized that one cannot generalize about the relative stability of exo- and endocyclic double bonds in 5-membered rings: *as far as the available experimental data are concerned, it seems that ordinarily an endo double bond in the 5-ring is at least as stable as an exo double bond in the 5-ring*. This statement was supported by two examples. The dehydration of 1-alkylcyclopentanols yields 1-alkylcyclopentenes [169] [(i) below], and an acid-catalyzed isomerization reaction transforms alkylidenecyclopentanes into 1-alkylcyclopentenes [169] [see (ii) below]:

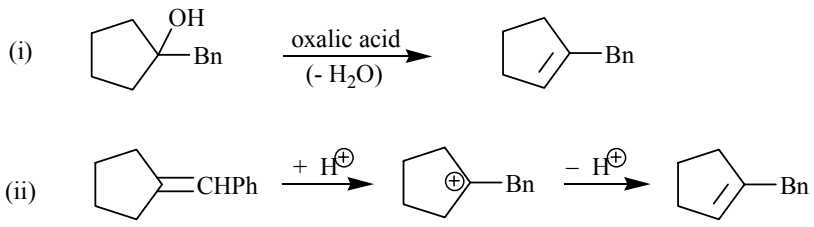

Brown responded [170] by stating that his hypothesis might be misinterpreted, i.e. the generalization ("Brown's hypothesis") can be misleading. He emphasized the importance of comparing the behaviour of any given set of 5- and 6-ring *analogues/derivatives* if this rule is to be applied. The statement was consequently re-phrased as follows: *Double bonds which are exo to a 5-ring are less reactive and more stable (relative to the saturated derivatives) than related double bonds which are exo to a 6-ring. Reactions which involve the formation or retention of an exo double bond in a 5-ring derivative will be favored over corresponding reactions which involve the formation or retention of an exo double bond in a 6-ring derivative. Reactions which involve the loss of an exo double bond will be favored in the 6-ring as compared to the corresponding 5-ring derivative.*

The intriguing difference in the stability and reactivity of exocyclic double bonds in five- and six-membered cyclic compounds has recently been observed in Michael's group during two different projects. In the most dramatic example, Michael *et al*. [171] found a spectacular difference in the outcome of an Eschenmoser sulfide contraction reaction of diethyl bromomalonate with the 5- and 6-membered 3-phenyl substituted thiolactams **321** and **322**, respectively, as shown in Scheme 77. Whereas the reaction proceeded as expected in the case of the 5-membered thiolactam **321** to afford vinylogous urethane **323** in 84% yield [after heating the intermediate thioimidate **324** at 60 °C in the presence of base (Scheme 77) to effect sulfur extrusion], reaction with the 6-membered thiolactam **322** afforded bicyclic thiazolidinone **325** in 66% yield, after heating the putative intermediate thioimidate **326** at 75 °C. Brown's hypothesis (see above) was therefore obeyed during these reactions. Whereas the 5-membered ring favoured the formation of an exocyclic double bond in **323**, the 6-membered ring reacted by an endocyclic deprotonation to favour the formation of an endocyclic double bond in product **325**.

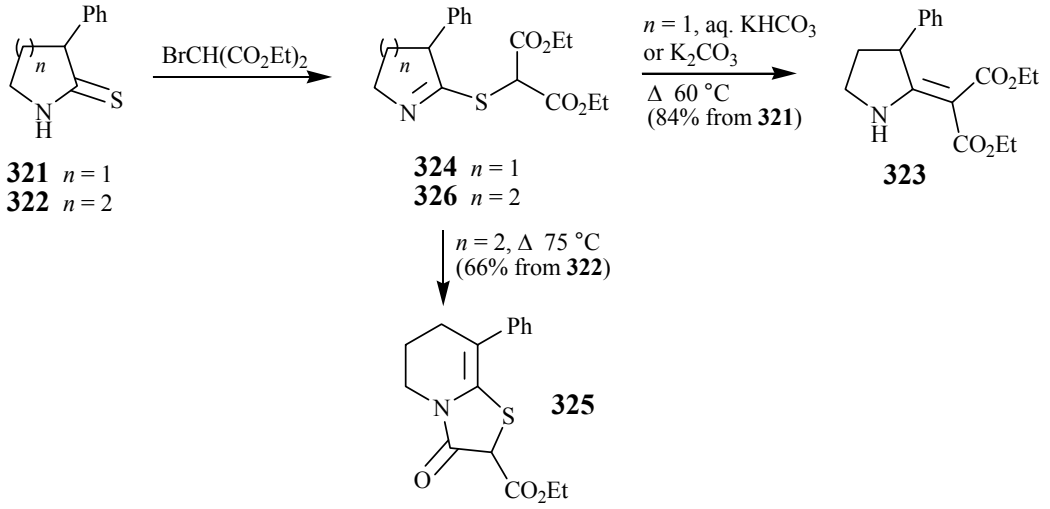

Scheme 77: The results obtained by Michael *et al*. [171].

Even when Michael *et al*. [171] prevented the formation of the endocyclic enamine in **332** by blocking the α-position with a second substituent, i.e. using thiolactam **327** instead in the Eschenmoser reaction, the formation of a vinylogous urethane still did not occur. Instead, thioisomünchnone **328** was obtained in 83% yield.

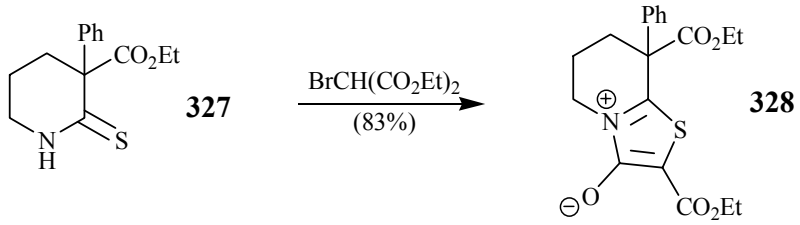

The second example observed in Michael's laboratory involved a difference in the sensitivity of 5- and 6-membered vinylogous urethanes towards reducing agents. The synthesis of (±)-lupinine [80] (also referred to before in Chapter 2, Figure 15, p. 52), the ester group in intermediate piperidinylidene vinylogous urethane **329** needed to be chemoselectively reduced to obtain the alcohol **330** (Scheme 78). Using standard reductive conditions (LAH, THF, rt), the major product obtained was ester **331**, i.e. reduction of both the saturated ester and the double bond of the vinylogous urethane had occurred. The desired enaminone **329** was obtained only in 3% yield. In contrast, when the analogous pyrrolidinylidene vinylogous urethane **332** was treated under the same conditions, the reaction was much more selective and **333** was obtained as the only product (Scheme 78). Although the yield of **330** could be improved in one trial

by reducing both the reaction temperature (to 0 ºC) and time (to 45 min), and in a second trial by also changing the solvent (to toluene:Et_2O, 2:1), the over-reduced side-product (**331**) was still isolated, albeit in lower yields (26% and 13%, respectively).

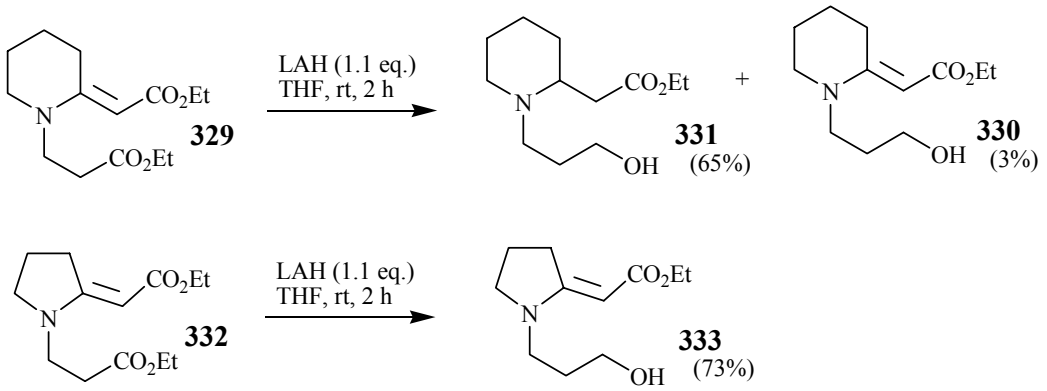

Scheme 78: The results obtained by Michael *et al*. [80] for the LAH reduction of **329** and **332** at rt.

It will be recalled that we experienced similar results in this project when attempting to reduce model pyrrolidinylidene (5-ring) vinylogous amides **143** (*N*-methyl protected), **147** [*N*-(2-cyanoethyl) protected] and **155** (free *N*H) chemoselectively (see Section 3.8.2., Table 9). Unfortunately, the quinazolinone residue in these compounds was also often reduced during the reduction trials, especially under harsher conditions, which resulted in complex mixtures of products. This made the purification, characterization and yield determination of the polar products very difficult. It was certainly apparent from the trials shown in Table 9, that the double bond in the enaminone groups of the 5-ring model compounds (**143**, **147** and **155**) resisted reduction under mild conditions, e.g. starting material was mostly recovered when **143** was subjected to hydrogenation over PtO_2 in AcOH. Furthermore, starting material was also the major compound isolated after attempting to reduce **155** using $NaBH(OAc)_3$ in AcOH-THF. In contrast, the hydrogenation of the model *N*-alkylated piperidinylidene (6-ring) vinylogous amides (**144**, **145** and **146**, Section 3.8.3), using PtO_2 in AcOH, occurred very efficiently to produce the desired synthetic alkaloids. The free N*H* piperidinylidene model compound **101** was also successfully reduced using PtO_2 and HCl in MeOH, albeit in modest yield, to afford deoxyfebrifugine (±)-**14**.

The disappointing results obtained during this project for the Eschenmoser reactions between 3-oxygen substituted piperidine-2-thiones and bromide **105** might also be explained using Brown's hypothesis. It was already mentioned, in Section 5.3.7., that dehydration of the intermediate thioiminium salt (formed in the reaction of 1-methyl-3-hydroxypiperidine-2-thione **315** with **105**, Scheme 74) might have occurred, which led to the formation of an aromatic product and/or decomposition. It could be argued that the resistance to the formation of double bond exocyclic to a six-membered ring had complicated this reaction. As Ma *et al*. [162] observed endocyclic double bond formation, in preference to the desired exocyclic double bond formation, during a similar reaction with an analogous pyrrolidine-2-thione (**305**, Scheme 73), we expect this to be even more likely to have occurred during our reaction with the 6-ring analogue. Similarly, in the reaction of 3-*O*Ac-substituted piperidine-2-thione **282** with **105** (Section 5.3.2., Scheme 67), dethionation of the intermediate thioiminium salt might have resulted from the preferential formation of an endocyclic double bond in the piperidine ring, which resulted in the formation of tetrahydrothiopyran **284**. The non-polar side-product, which results from elimination in the piperidine ring, possibly was not isolated owing to its presence in an inseparable mixture of non-polar products (PPh_3 etc.), which eluted during column purification. This therefore represents an alternative but speculative mechanism to that given in Scheme 68 for the formation of **284**.

A comparative single crystal X-ray diffraction study, and a correlation with NMR data, of cyclic enaminones of varying ring size might improve our understanding of the difference in reactivity and stability of the exocyclic double bonds in these compounds. In this chapter, we will discuss and compare the crystal structures, in addition to the other characterization data obtained, of various model cyclic vinylogous amides synthesized as discussed in Chapter 3. To our knowledge, no crystal structures of either febrifugine (**1**) or deoxyfebrifugine (**14**) analogues have been published before.

6.2. Crystal structures of selected model vinylogous amides

6.2.1. (2*E*)-2-(1-Methylpiperidin-2-ylidene)-1-phenylethanone (172)

In a related project conducted in our laboratory [83], phenyl substituted enaminone **172**

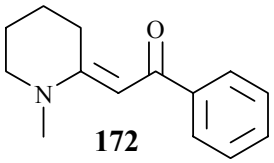

172

was synthesized in order to test and to optimize the pivotal selective C=C reduction reaction mentioned above in Section 6.1.3. The mild conditions (H_2, PtO_2, AcOH), which the *N*-alkylated model enaminones (Section 3.8.3.) were subjected to before, were also found to be successful for the selective reduction of **172** to afford natural product [172] (±)-sedaminone (**173**). The use of HCl and MeOH as solvent, instead of AcOH, also led to the formation of **173** as the only product. These were satisfying results since, even though **173** had been synthesized before using Eschenmoser methodology (see Scheme 35, Section 3.8.1.), Pt hydrogenation had never been used for the conversion of **172** into **173**. The ketone group in **172** is expected to be sensitive to these hydrogenation conditions, owing to a weakening of the C=O bond by the electron-withdrawing phenyl substituent. However, we observed no evidence of the formation of the over-reduced products, (±)-sedamine **170** and (±)-allosedamine **171** (see Scheme 35, Section 3.8.1.), under these reaction conditions. During this Ph.D. project, we re-synthesized **172** in order to obtain single crystals for structure determination. We wanted to compare the structure of an enaminone group bearing an electron-withdrawing aryl substituent (such as that found in **172**) with the structures of our model enaminones, which are alkyl substituted on the enaminone group.

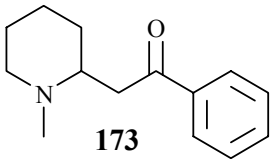

173

The important crystal and refinement data for **172** are given in Table 25.

Crystal system	Monoclinic	
Space group	$P2_1/c$	
Unit cell dimensions	a = 8.006(2) Å	α = 90°.
	b = 9.441(3) Å	β = 95.197(6)°.
	c = 15.535(4) Å	γ = 90°.
Volume	1169.5(6) Å^3	

Z	4
Density (calculated)	1.223 Mg/m^3
Absorption coefficient	0.077 mm^{-1}
F(000)	464
Crystal size	0.38 x 0.28 x 0.24 mm^3
Theta range for data collection	2.53 to 27.99°.
Index ranges	-10<=*h*<=10, -9<=*k*<=12, -20<=*l*<=15
Reflections collected	6125
Independent reflections	2829 [*R*(int) = 0.0394]
Completeness to theta = 27.99°	99.9 %
Absorption correction	None
Refinement method	Full-matrix least-squares on F^2
Data / restraints / parameters	2829 / 38 / 167
Goodness-of-fit on F^2	0.997
Final *R* indices [*I*>2sigma(*I*)]	*R*1 = 0.0551, *wR*2 = 0.1584
R indices (all data)	*R*1 = 0.0926, *wR*2 = 0.2090
Largest diff. peak and hole	0.309 and -0.364 $e.Å^{-3}$

Table 25: Selected crystal and refinement data for **172**.

An Ortep diagram of **172** is shown in Figure 29. It can be seen that disorder was found in the piperidinylidene ring at carbons 3, 4, 5 and 6. These atoms were refined over two positions (A and B). In both structures (A and B), the ring is in the half-chair conformation, with carbons 4 and 5 being out-of-plane with the other ring atoms. It is clear from Figure 29 that **172** crystallized in the expected *E*-configuration about the enaminone C=C bond. Steric repulsion between the *N*-methyl group and the enaminone carbonyl group favours the *E*-configuration.

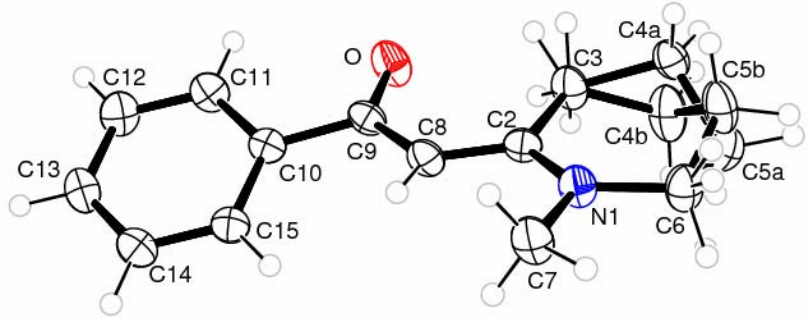

Figure 29: Ortep diagram of **172** (showing 50% ellipsoid probability), indicating the disorder found in the piperidinylidene ring.

6.2.2. 3-{(2*E*)-2-[2-Oxo-3-(4-oxoquinazolin-3(4*H*)-yl)propylidene]piperidin-1-yl}propanenitrile (146)

The crystal structure of the *N*-(2-cyanoethyl) model vinylogous amide **146** was particularly interesting seeing that **146** crystallized in the noncentrosymmetric space group $P2_1$. The important crystal and refinement data for **146** are given in Table 26.

Crystal system	Monoclinic	
Space group	$P2_1$	
Unit cell dimensions	a = 8.7000(10) Å	α = 90°.
	b = 8.9029(11) Å	β = 98.920(2)°.
	c = 10.9921(13) Å	γ = 90°.
Volume	841.10(17) Å^3	
Z	2	
Density (calculated)	1.328 Mg/m^3	
Absorption coefficient	0.089 mm^{-1}	
F(000)	356	
Crystal size	0.48 x 0.35 x 0.15 mm^3	
Theta range for data collection	1.88 to 25.98°.	
Index ranges	-10<=h<=10, -10<=k<=10, -13<=l<=9	
Reflections collected	5054	
Independent reflections	3187 [R(int) = 0.0152]	
Completeness to theta = 25.98°	99.9 %	
Absorption correction	None	
Refinement method	Full-matrix least-squares on F^2	
Data / restraints / parameters	3187 / 7 / 240	
Goodness-of-fit on F^2	1.021	
Final R indices [I>2sigma(I)]	R1 = 0.0416, wR2 = 0.1014	
R indices (all data)	R1 = 0.0544, wR2 = 0.1092	
Absolute structure parameter	2.2(14)	
Largest diff. peak and hole	0.177 and -0.257 e.Å^{-3}	

Table 26: Selected crystal and refinement data for **146**.

An Ortep diagram of **146** is shown in Figure 30. It can be seen that disorder was again encountered in C2′, C3′, C4′ and C5′ of the piperidinylidene ring of **146**. These carbons were consequently refined over two positions as before (A and B). Although not clearly apparent in Figure 30 (but perhaps more so in Figure 31 below), the piperidinylidene 6-membered rings in both refinements A and B resemble more closely the "sofa" conformation rather than the half-chair conformation observed for the other piperidinylidene model compounds. Carbon atom C4′ is much more out-of-plane than C3′ is with the other ring atoms. The torsion angles are compared in Section 6.4. The quinazolinone residue is rotated so that the two oxygen atoms, O1 and O2, are far apart in space. The 2-cyanoethyl group on nitrogen is in a *gauche syn* conformation about the C7′-C8′ bond, the torsion angle N1′-C7′-C8′-C9′ being 63.7 (3) º.

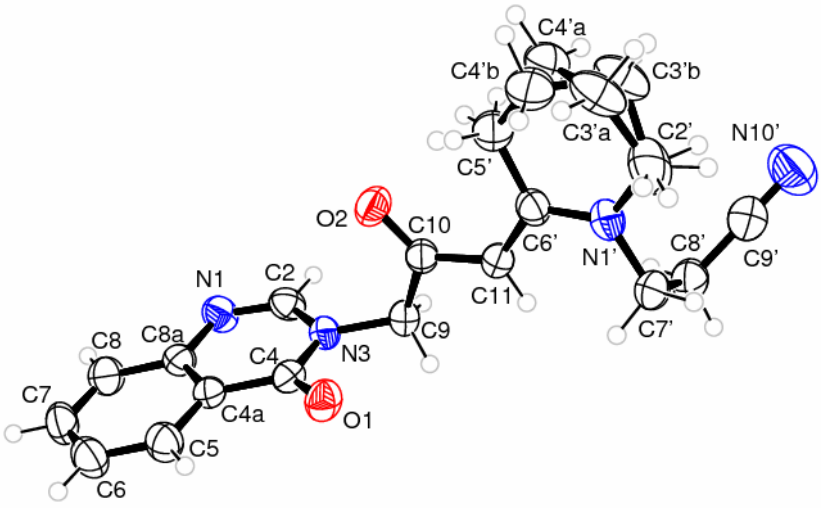

Figure 30: Ortep diagram (showing 50% ellipsoid probability) of **146**, indictating disorder in the piperidinylidene ring.

The unit cell in structure **146** is represented in Figure 31. It can be seen that the two molecules constituting the asymmetric unit are not related to each other by any inversion centres or reflection planes, but by a two-fold screw axis. The two molecules shown are therefore superimposable by translation, followed by rotation through 180º. The molecule is therefore chiral and crystallized as an enantiopure compound, even though there is no asymmetric carbon in **146**. This result is discussed further when the structures of **146** and analogue **101** (Section 6.2.3. below) are compared in Section 6.3.

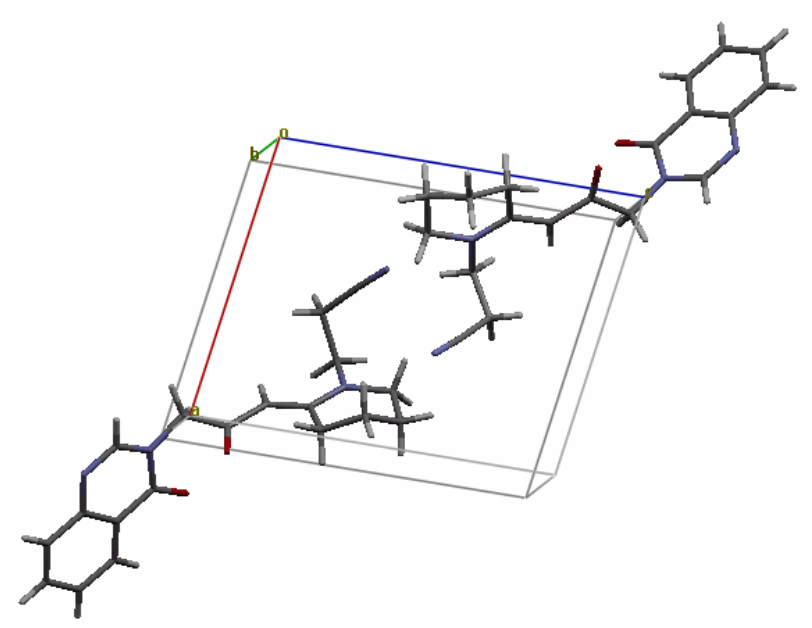

Figure 31: A unit cell representation of **146**, with disorder removed for clarity.

6.2.3. 3-[(3*Z*)-2-Oxo-3-(piperidin-2-ylidene)propyl]quinazolin-4(3*H*)-one (101)

Selected crystal and refinement data for **101** are given in Table 27.

Crystal system	Monoclinic	
Space group	$P2_1/c$	
Unit cell dimensions	a = 14.2954(19) Å	α = 90°.
	b = 5.2528(7) Å	β = 92.069(3)°.
	c = 18.970(3) Å	γ = 90°.
Volume	1423.6(3) Å^3	
Z	4	
Density (calculated)	1.329 Mg/m^3	
Absorption coefficient	0.089 mm^{-1}	
F(000)	600	
Crystal size	0.26 x 0.20 x 0.10 mm^3	
Theta range for data collection	1.43 to 25.99°.	
Index ranges	-17<=h<=16, -6<=k<=6, -23<=l<=22	

Reflections collected	8038
Independent reflections	2806 [R(int) = 0.0297]
Completeness to theta = 25.99°	100.0 %
Absorption correction	None
Refinement method	Full-matrix least-squares on F^2
Data / restraints / parameters	2806 / 30 / 216
Goodness-of-fit on F^2	1.012
Final R indices [I>2sigma(I)]	$R1$ = 0.0457, $wR2$ = 0.1194
R indices (all data)	$R1$ = 0.0807, $wR2$ = 0.1370
Extinction coefficient	0.011(2)
Largest diff. peak and hole	0.159 and -0.133 e.Å^{-3}

Table 27: Selected crystal and refinement data for **101**.

An Ortep diagram of **101** is given in Figure 32. Again disorder was encountered in the piperidinylidene residue and treated as before. The two refined piperidinylidene rings (A and B) are in half-chair conformations. It is clear from Figure 32 that the enaminone group is in the expected *Z*-configuration about the C=C (C6′-C11) bond, owing to the stabilizing effect of intramolecular hydrogen bonding between N1′(donor)···O2(acceptor).

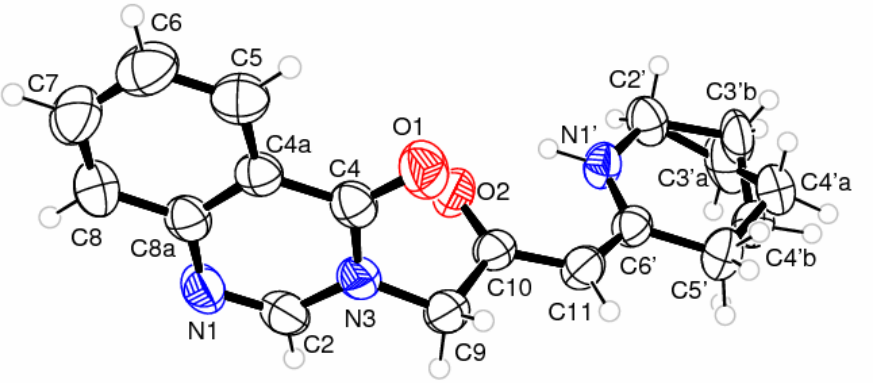

Figure 32: Ortep diagram (showing 50% ellipsoid probability) of **101**, indicating disorder.

Figure 33 represents a unit cell in structure **101**. It can be seen that the intermolecular hydrogen bonds are formed along the *a*-axis of the crystal, and the molecules are also aligned along this axis. The molecules are stacked on top of each other in a regular pattern such that complementary close interactions are formed between the electron-rich quinazolinonone residues and the electron-poorer piperidinylidene moieties.

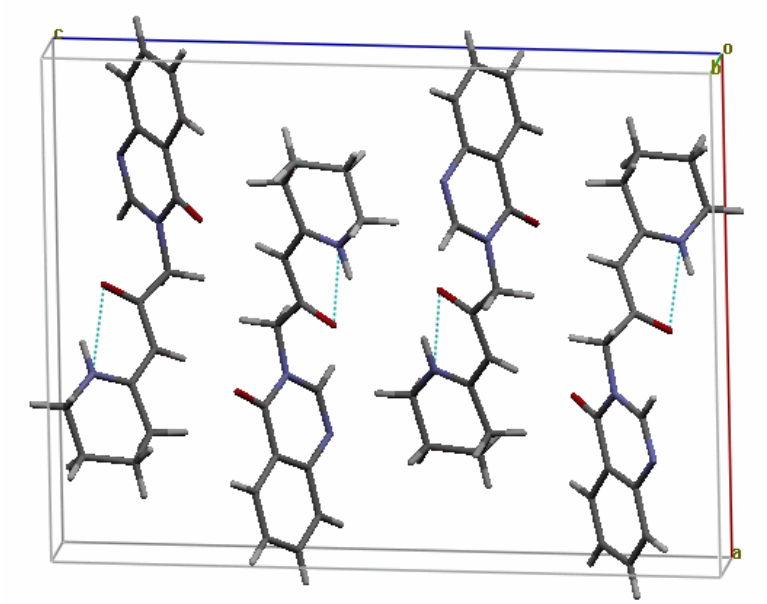

Figure 33: Unit cell representation (with disorder removed for clarity) of **101**. (As mentioned before in Section 4.2.2., because the hydrogen atoms were placed during structure refinement, the hydrogen bonds are shown between the hydrogen bond donor and acceptor atoms)

6.2.4. 3-[(3*Z*)-2-Oxo-3-(pyrrolidin-2-ylidene)propyl]quinazolin-4(3*H*)-one (155)

Selected crystal and refinement data for structure **155** are given in Table 28.

Crystal system	Monoclinic	
Space group	$P2_1/c$	
Unit cell dimensions	a = 14.217(2) Å	α = 90°.
	b = 5.2266(8) Å	β = 92.521(3)°.
	c = 18.098(3) Å	γ = 90°.

Volume	1343.5(4) Å^3
Z	4
Density (calculated)	1.331 Mg/m^3
Absorption coefficient	0.091 mm^{-1}
F(000)	568
Crystal size	0.50 x 0.18 x 0.04 mm^3
Theta range for data collection	1.43 to 26.00°.
Index ranges	-17<=*h*<=17, -6<=*k*<=6, -22<=*l*<=17
Reflections collected	7436
Independent reflections	2650 [*R*(int) = 0.0376]
Completeness to theta = 26.00°	99.7 %
Absorption correction	None
Refinement method	Full-matrix least-squares on F^2
Data / restraints / parameters	2650 / 22 / 198
Goodness-of-fit on F^2	1.013
Final *R* indices [*I*>2sigma(*I*)]	*R*1 = 0.0666, *wR*2 = 0.1700
R indices (all data)	*R*1 = 0.1341, *wR*2 = 0.2160
Extinction coefficient	0.040(6)
Largest diff. peak and hole	0.329 and -0.317 e.Å^{-3}

Table 27: Selected crystal and refinement data for **155**.

An Ortep diagram of **155** is given in Figure 34. In this structure, the 5-membered pyrrolidinylidene ring showed disorder with respect to C3′. This carbon was refined over two positions (A and B), which corresponded to two envelope conformations of the ring, C3′ being out-of-plane with the other ring atoms. The *Z*-configuration was again observed in the enaminone group.

Figure 35 represents a unit cell in structure **155**. It can be seen that the molecular packing in **155** is very similar to that described for **101** above. However, another pair of hydrogen bonds, in addition to the intramolecular hydrogen bonds, is formed intermolecularly between adjacent N1′ and O2 atoms, resulting in dimerization. This is because the five-membered ring in **155** takes up less space than the corresponding

6-membered ring in analogue **101**, which allows for closer contact between molecules along the *a*-axis in **155** so that tandem hydrogen bonds can form. The distance between N1′ and O2 (i.e. 2.967 Å) of adjacent molecules now falls within the range accepted (i.e. shorter than 3.0 Å) for a formal, classified hydrogen bond. The corresponding intermolecular N1′·····O2 distance in structure **101** is much longer (5.441 Å), even though the intermolecular interaction patterns are very similar in **155** and **101**.

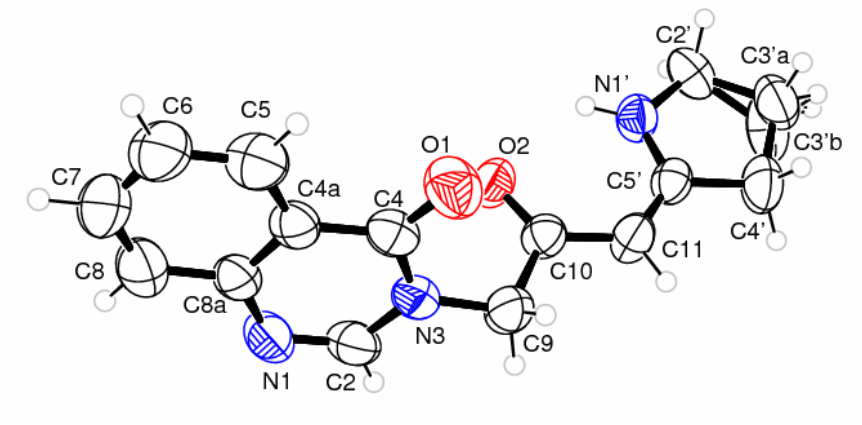

Figure 34: Ortep diagram (showing 50% ellipsoid probability) of **155**, indicating disorder.

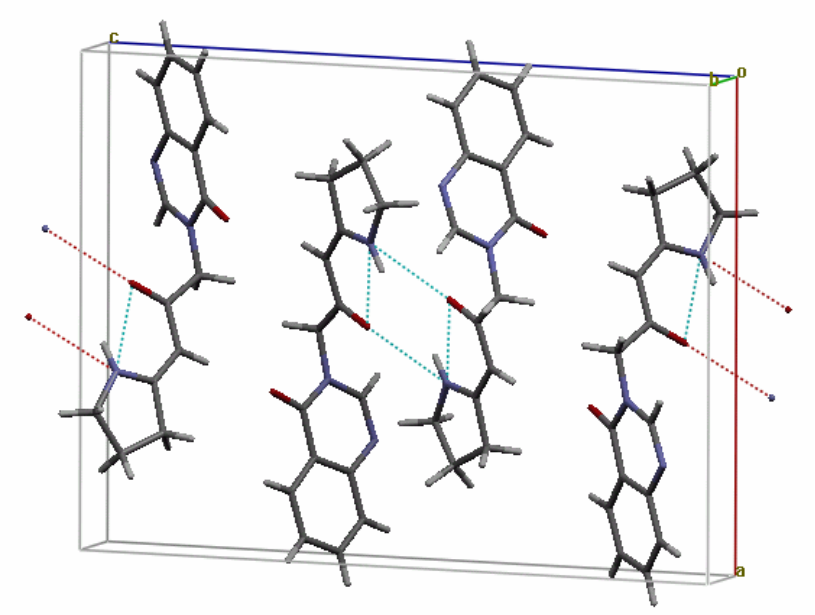

Figure 35: Unit cell representation (with disorder removed for clarity) of **155**.

6.2.5. 3-[(3*Z*)-3-(Azepan-2-ylidene)-2-oxopropyl]quinazolin-4(3*H*)-one (156)

Selected crystal and refinement data for structure **156** are given in Table 28.

Crystal system	Monoclinic	
Space group	$P2_1/c$	
Unit cell dimensions	a = 10.2040(14) Å	α = 90°.
	b = 14.719(2) Å	β = 93.130(3)°.
	c = 10.0480(15) Å	γ = 90°.
Volume	1506.9(4) Å^3	
Z	4	
Density (calculated)	1.311 Mg/m^3	
Absorption coefficient	0.088 mm-1	
F(000)	632	
Crystal size	0.32 x 0.26 x 0.14 mm^3	
Theta range for data collection	2.00 to 26.00°.	
Index ranges	-12<=h<=9, -17<=k<=18, -12<=l<=12	
Reflections collected	8848	
Independent reflections	2960 [R(int) = 0.0377]	
Completeness to theta = 26.00°	99.9 %	
Absorption correction	Semi-empirical from equivalents	
Max. and min. transmission	0.9878 and 0.9724	
Refinement method	Full-matrix least-squares on F^2	
Data / restraints / parameters	2960 / 0 / 199	
Goodness-of-fit on F^2	1.077	
Final R indices [I>2sigma(I)]	R1 = 0.0577, wR2 = 0.1601	
R indices (all data)	R1 = 0.1035, wR2 = 0.1792	
Largest diff. peak and hole	0.528 and -0.204 e.Å^{-3}	

Table 28: Selected crystal and refinement data for **156**.

An Ortep diagram of **156** is given in Figure 36. In this structure, the 7-membered azepanylidene ring of **156** is in the most stable chair conformation. Carbons C7′, C6′ and C3′ are out-of-plane with the other 4 ring atoms. Interestingly, no disorder was observed in the azepanylidene ring of **156**, in contrast to the smaller 6- and 5-membered rings discussed before in the structures of **172**, **146**, **101** and **155**. The *Z*-configuration in the enaminone group of **156** is again apparent, owing to intermolecular hydrogen bonding.

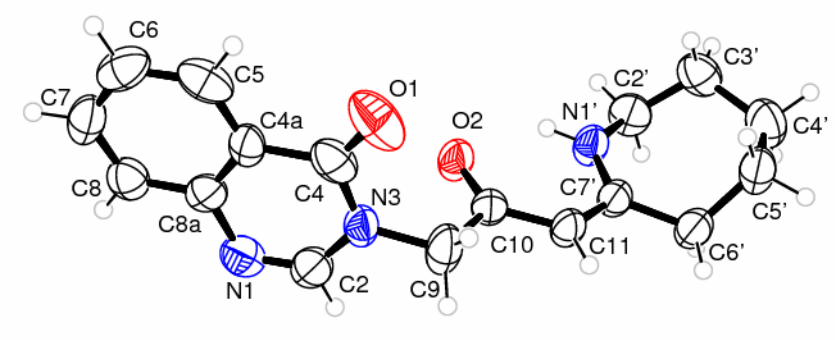

Figure 36: Ortep diagram (showing 50% ellipsoid probability) of **156**.

Figure 37 represents a unit cell in structure **156**. It can be seen that the molecular packing in **156** is less ordered than in analogues **101** and **155**. The larger 7-membered ring in **156** prevents the intimate and well-aligned intermolecular associations observed in **101** and **155**.

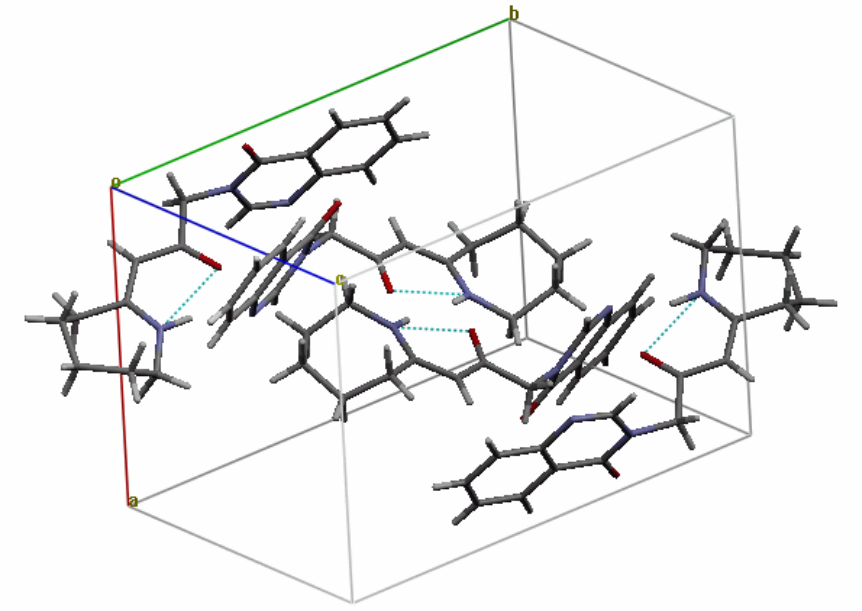

Figure 37: Unit cell representation of **156**.

6.2.6. 3-[(3*Z*)-3-(Azocan-2-ylidene)-2-oxopropyl]quinazolin-4(3*H*)-one (157)

Selected crystal and refinement data for structure **157** are given in Table 29.

Crystal system	Monoclinic	
Space group	$P2_1/n$	
Unit cell dimensions	a = 13.581(3) Å	α = 90°.
	b = 5.1506(9) Å	β = 95.376(3)°.
	c = 22.272(4) Å	γ = 90°.
Volume	1551.1(5) Å^3	
Z	4	
Density (calculated)	1.333 Mg/m^3	
Absorption coefficient	0.089 mm^{-1}	
F(000)	664	
Crystal size	0.38 x 0.18 x 0.08 mm^3	
Theta range for data collection	1.69 to 26.00°.	
Index ranges	-14<=h<=16, -6<=k<=6, -25<=l<=27	
Reflections collected	8255	
Independent reflections	3037 [R(int) = 0.0400]	
Completeness to theta = 26.00°	99.4 %	
Absorption correction	None	
Refinement method	Full-matrix least-squares on F^2	
Data / restraints / parameters	3037 / 0 / 208	
Goodness-of-fit on F^2	1.021	
Final R indices [I>2sigma(I)]	R1 = 0.0432, wR2 = 0.0907	
R indices (all data)	R1 = 0.0740, wR2 = 0.1006	
Largest diff. peak and hole	0.161 and -0.186 e.Å^{-3}	

Table 28: Selected crystal and refinement data for **157**.

An Ortep diagram of **157** is given in Figure 38. In this structure, the 8-membered azecanylidene ring of **157** is in the most stable boat-like conformation. Although not very clear in Figure 38, carbons C2′, C3′, C5′, C6′ and C7′ lie approximately in the

same plane, with C4′, C8′ and N1′ projecting to the same side and out of this plane. Surprisingly, similar to the case for **156** above, no disorder was encountered in the relatively large 8-membered ring.

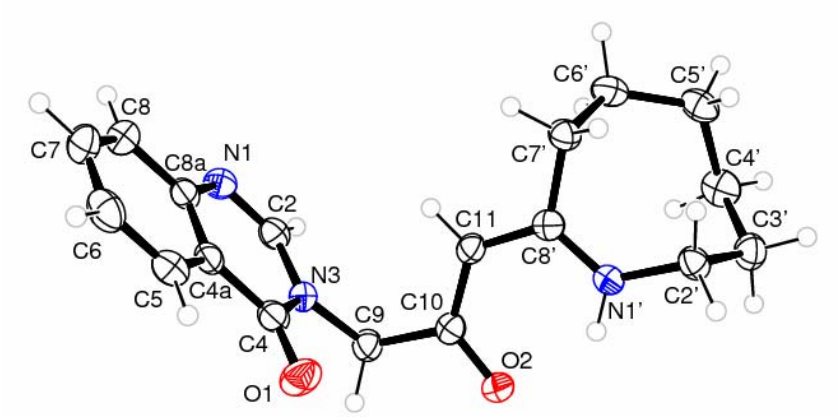

Figure 38: Ortep diagram (showing 50% ellipsoid probability) of **156**.

Figure 39 represents a unit cell in structure **157**. It can be seen that the large size of the 8-membered ring in **157**, as was the case for **156**, causes significant internal torsion of the two parts (quinazolinone and azocanylidene ring) of the molecule with respect to each other. This also results in a less flat (or sheet-like) molecular packing pattern than in **101** and **155**. Interestingly, tandem intermolecular hydrogen bonds (of magnitude 2.964 Å) are again observed in **157**, similar to those in the pyrrolidinylidene analogue **155** (of magnitude 2.965 Å, see Section 6.2.4.). Furthermore, the intermolecular O2···O2 distance in the dimers of **157** is surprisingly short (3.032 Å, see Figure 39) as a result of these tandem hydrogen bonds. This distance is considerably shorter than the corresponding distance in **155** (3.471 Å). This can be explained by the relatively larger size of the 8-membered ring in **157**, compared to the 5-membered ring in **155**, which forces N1 and O2 closer together intramolecularly. This is discussed further in Section 6.5., when the hydrogen bonds are compared in the secondary enaminone model compounds.

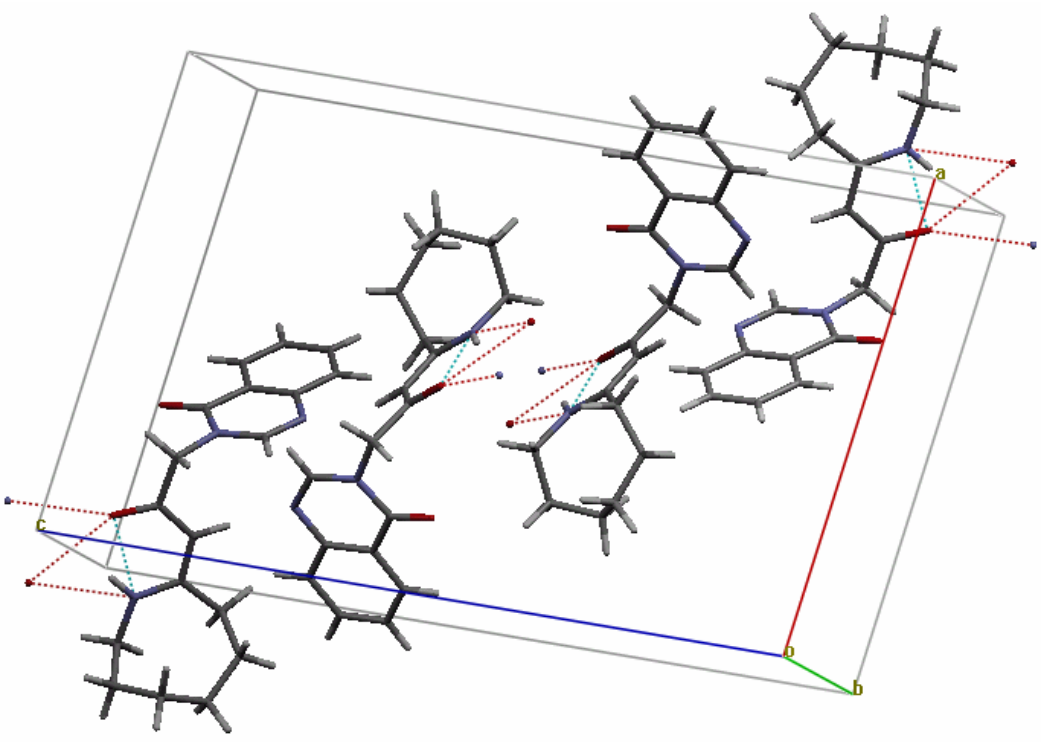

Figure 39: Unit cell representation of **157**.

6.3. Comparison of crystal structures and physical properties

Most of the model enaminones discussed in Section 6.2. crystallized in one of the most common crystal systems and space groups found for organic crystals, i.e. the monoclinic $P2_1/c$ group, with the exception of **146** (monoclinic $P2_1$) and **157** (monoclinic $P2_1/n$).

The melting points and R_f-values obtained for the model enaminones discussed here are compared in Table 29. It can be seen that the quinazolinone residue greatly increases the polarities and melting points of the deoxyfebrifugine analogues (**146**, **101**, **155**, **156**, **157**) compared to the phenyl-substituted derivative **172**. The melting points and the polarities of the quinazolinone-based compounds do not follow exactly the expected trends. The pyrrolidinylidene analogue **155** is expected to exhibit a relatively high melting point, which is the case, as a result of the additional intermolecular hydrogen bonds found in its structure. However, these intermolecular bonds were also observed in structure **157**, which melts at the lowest temperature in

the quinazolinone series. It is thought that the relatively large 8-membered ring (with an increased nonpolar hydrocarbon component) in **157** reduces the extent of close packing for steric reasons and is the primary cause for lowering the melting point of **157** compared to its analogues. The melting point of the azepanylidene analogue **156** is unexpectedly high, even though it is the least polar compound (by R_f-value) in the quinazolinone series. One reason could be that no disorder was observed, as for the 5- and 6-membered cyclic analogues, in the azepanylidene ring of **156**. Although the melting point of the piperidinylidene analogue **101** (167.5-170 ºC) is a bit lower than that obtained for the compound isolated by Baker's group during their second synthesis (176-178 ºC; the first crop of crystals they obtained had a melting point of 167-170 ºC) [66], we are certain that these two compounds are the same and possess the structure of **101**, as discussed in Section 1.7.2.

compound	R_f-value (and eluent)	Melting point (ºC)
172	0.36 (EtOAc:hexane, 1:1)	67-70
146	0.15 (EtOAc)	179-180
101	0.18 (EtOAc:hexane, 4:1)	167.5-170
155	0.17 (EtOAc)	181-182
156	0.47 (EtOAc)	201.5-203
157	0.33 (EtOAc)	149-150

Table 29: Comparison of R_f-values and melting points obtained for the model enaminones.

The melting point of **146** is higher than that of the analogous compound **101**, owing to closer molecular packing in the structure of **146**. As mentioned before, **146** crystallizes as an enantiomerically pure crystal, which is unusual for an inherently non-chiral molecule. It is thought that the presence of the electron-rich 2-cyanoethyl group forces this molecule to crystallize in this way. It has been known for a long time that the primary packing rule for molecular crystals is the maximizing of intermolecular contact and the minimizing of the volume per molecule [173]. This is further elaborated upon by Kitaigorodskii's "bumps and hollows" principle [174], which states that a "bump" in one molecule will associate with a "hollow" in its neighbour

so that intermolecular contact can be maximized. In other words, molecular complementarity and self-complementarity govern the packing patterns in molecular crystals. “Complementarity” refers to the association of, e.g. hydrophobic groups in a molecule with hydrophobic groups in other molecules, or the attraction of electron-rich parts in a molecule to electron-poor parts in other molecules. During the crystallization of **146**, it seems possible that the highly electron-rich cyanoethyl groups might reduce the extent of close association between “two enantiomorphs”, in which the cyanoethyl groups point towards each other, by electrostatic repulsion. Closer packing in **146** is therefore facilitated by the growth of a chiral crystal, i.e. the cyanoethyl groups can be further apart from each other when the crystal grows in a chiral manner. The resulting solid structure of **146** is therefore less symmetrical than that of the less sterically challenged analogue **101** (see Sections 6.2.2. and 6.2.3.), but multiple close intermolecular contacts are ensured between complementary regions in **146**. Chandrakantha’s group published the structures of two *N*-(2-cyanoethyl) group containing indoles, **327** in 1990 [175] and **328** in 1999 [176].

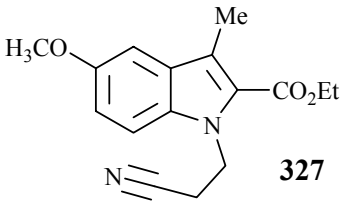

327

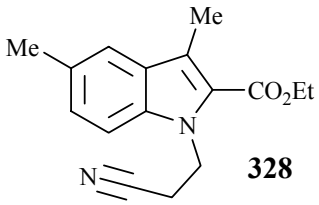

328

They found that substitution of the indole nitrogen by the 2-cyanoethyl group to obtain **327** brought about a remarkable change in crystal packing [176]. This is similar to what we observed when comparing the packing in structure **146** with that in **101**, although they did not observe a change in space group, and the crystal of **327** was still centrosymmetric. Tabulated below is a comparison of bond lengths and bond angles between **327** and **146**, based on our numbering scheme:

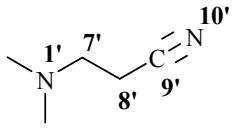

It can be seen from Table 30 (third column) that two molecules were found in the asymmetric unit of **327**. The bond parameters in the cyanoethyl group of **146** generally correspond best to those in the *second* molecule of **327**. However, the presence of the electron-withdrawing cyano group has less influence on the bond lengths in **327** than in **146**. The C7′-C8′ bond in **146** is longer, and the C8′-C9′ bond is considerably shorter in **146**, than that observed for both molecules of **327**. The C≡N

(C9′-N10′) bond length is also longer (1.143 Å) in **146** than that found for the molecules in **157** (1.087 and 1.114 Å, respectively). The average magnitude for a C*-C≡N bond is 1.136 Å [127], therefore the nitrile triple bond in **146** is closer to the ideal magnitude.

Bond (Å)	**146**	**327** (two molecules)
N1′-C7′	1.464(3)	1.516(9), 1.460(7)
C7′-C8′	1.523(4)	1.424(9), 1.502(8)
C8′-C9′	1.458(4)	1.645(11), 1.503(9)
C9′-N10′	1.143(3)	1.087(9), 1.114(9)
Angle (degrees)	**146**	**327**
N1′-C7′-C8′	109.1	101.0(6), 108.7(5)
C7′-C8′-C9′	111.2(2)	103.1(6), 108.8(5)
C8′-C9′-N10′	177.0(3)	168.7(8), 177.8(7)

Table 30: Comparison between structures **146** and **327**.

Phenyl-substituted enaminone **172** crystallizes as a practically planar molecule, as seen in Figure 29 (Section 6.2.1.). In contrast, it can be seen from the diagrams in Section 6.2. that all the quinazolinone-containing enaminones basically consist of two structural entities, the enaminone ring and the quinazolinone ring, which lie in two different planes as a result of torsion in the linking central ketone chain. Figure 40 illustrates how the incline between these two planes increases as the enaminone ring size increases. The incline is approximately 45º in the 5-ring analogue **155**, as well as the *N*-2-cyanoethyl protected 6-ring analogue **146**, it then increases slightly over the free *N*H 6-ring (**101**) and 7-ring (**156**) analogues (the angle being almost the same in the latter two). Then a drastic increase to an approximately 90º angle between these two planes is observed for 8-ring analogue **157**. Another important difference in the structure of **157** is apparent in Figure 40. Whereas the ketone oxygen in the enaminones of all the other derivatives is *syn* to the quinazolinone residue, this oxygen becomes approximately *anti* to the quinazolinone residue in **157**. The differences observed here for **157** are attributed to the presence of the larger 8-membered ring in **157**. The 7- to 8-membered ring transition in this series causes a

sudden obvious change in the crystalline conformation, owing to space limitations in the 8-ring compound. This could also explain the unexpectedly low melting point of **157**, mentioned above, since less dense packing can occur in **157**.

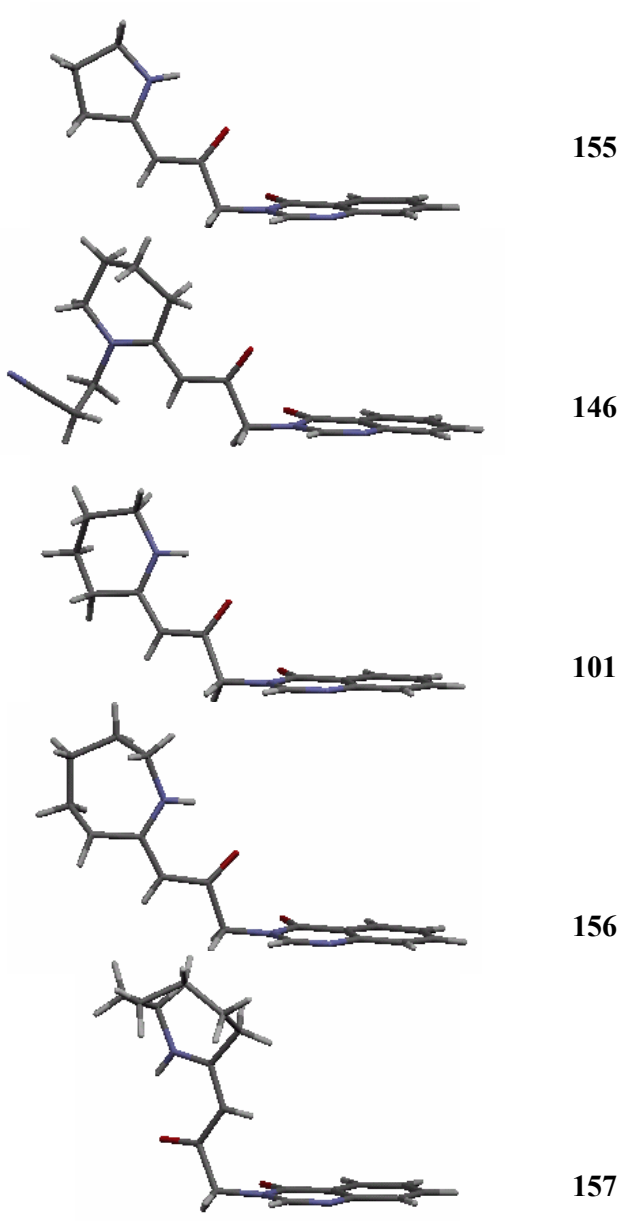

Figure 40: Comparison of the planar incline in the quinazolinone enaminones.

6.4. Comparison of torsion angles

As we were particularly interested in the conformations of the enaminone functional groups of the model compounds, we will focus only on these groups during the

remainder of the chapter. Note that, for comparative purposes, we will use the numbering scheme given in Figure 41 and only concentrate on the atoms numbered here throughout the remainder of this chapter. Hydrogens are numbered according to the carbon or the nitrogen they are bonded to. Therefore, we shall only deal with the following atoms: N1′ (and H1′ if present), C2′, C*x*, C*y*, C9, C10, C11 and O2. This numbering scheme was chosen because all of the structures, except that of phenyl-substituted enaminone **172**, are numbered the same with respect to atoms N1′, C2′, C9, C10, C11 and O2. For **172**, all the atomic numbers are unfortunately changed, but it is easy enough to correlate the numbers given in the Ortep diagram of **172** (Figure 29) with the ones given below. For the other five structures (in the quinazolinone series), the correlations with C*x* and C*y* are given in Table 31.

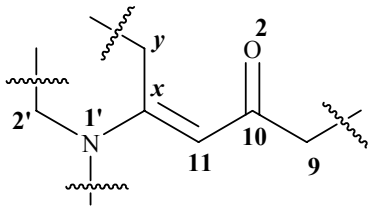

Figure 41: Generalized enaminone numbering scheme applied to all the structures in this chapter.

Compound	*x*	*y*
146	6′	5′
101	6′	5′
155	5′	4′
156	7′	6′
157	8′	7′

Table 31: Correlation of generalized numbering scheme (C*x* and C*y*) with the appropriate carbons in the quinazolinone series.

Compared in Table 31 are selected torsion angles in the enaminone groups of the model vinylogous amides. It can be seen from these torsion angles, which are all within *ca*. 6º of either (±) 0º or (±) 180º, that the enaminone groups in all cases are practically planar because N1′, C*x*, C11 and C10 are all sp^2-hybridized, which forces

planarity in this group. Perhaps worth mentioning is the slight deviation from planarity with the enaminone group of carbons C2′ and C*y* (i.e. C5′) in the piperidinylidene ring of the cyanoethyl derivative **146**, as reflected by the C11-C*x*-N1′ -C2′ and C10-C11-C*x*-C*y* torsion angles. This is probably again a reflection of the steric hindrance caused by the cyanoethyl substituent in **146**, which causes slight deviations from the ideal during close molecular packing.

torsion angle	**172**	**146**	**101**	**155**	**156**	**157**
C10-C11-C*x*-N1′	-178.52 (18)	174.9 (2)	2.3(3)	1.7(5)	4.2(4)	-1.6(3)
O2-C10-C11-C*x*	4.8(3)	-0.5 (4)	-3.7(3)	0.1(5)	-0.5(4)	-2.0(3)
C11-C*x*-N1′-C2′	171.43 (18)	-174.3(2), 6.7(3)	178.44 (17)	-178.0 (3)	176.3 (3)	-179.64 (16)
C10-C11-C*x*-C*y*	1.6(3)	-6.1(3)	-176.63 (17)	-175.5 (3)	-174.7 (3)	178.50 (16)

Table 31: Comparison of torsion angles (in degrees).

6.5. Comparison of interatomic distances and bond angles

Selected interatomic distances (including hydrogen bonds) are compared in Table 32 (with the generalized numbering scheme given again above the table). Electronic delocalisation in the enaminone groups of all these compounds is reflected in the bond lengths. Selected average bond lengths between sp^2-hybridized atoms, in which the double bonds are conjugated, are given in Table 33 [127]. There are no average bond lengths given for the enaminone functional group in the crystallographic reference tables [127], as this is a rather uncommon group. Table 33 therefore also gives the description of the corresponding “enaminone” bond, to which we might compare the conjugated bond lengths given.

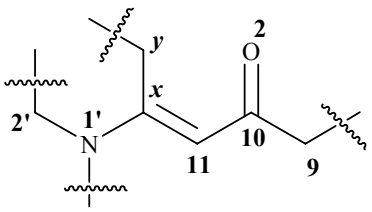

inter-atomic distance	**172**	**146**	**101**	**155**	**156**	**157**
N1′-H1′	n.a.	n.a.	0.923(19)	0.86(3)	0.860(0)	0.880(0)
N1′-C*x*	1.349(2)	1.360(3)	1.329(2)	1.317(4)	1.331(3)	1.327(2)
C*x*-C11	1.394(3)	1.374(3)	1.382(2)	1.364(4)	1.380(3)	1.402(2)
C11-C10	1.425(3)	1.429(3)	1.405(2)	1.401(4)	1.415(3)	1.409(2)
C10-O2	1.254(2)	1.235(2)	1.248(2)	1.242(3)	1.242(3)	1.250(2)
O2-N1′	n.a.	n.a.	2.737(2)	2.792(3)	2.711(3)	2.704(0)
O2-H1′	n.a.	n.a.	2.020	2.250	2.035	2.011
N1′-C2′	1.470(3)	1.472(3)	1.458(2)	1.458(4)	1.464(3)	1.454(2)
C*x*-C*y*	1.507(2)	1.498(3)	1.507(2)	1.507(4)	1.507(3)	1.507(2)
C10-C9	n.a.	1.530(3)	1.533(2)	1.528(4)	1.526(4)	1.530(2)

Table 32: Comparison of selected interatomic distances in the enaminone groups. (n.a. = not applicable)

bond description	average length (Å)	Corresponding bond in enaminone
$(C^{\#})_2$–**N**–**C**=C, (N sp^2 planar)	1.355	N1′-C*x* (in **172** and **146**)
$C^{\#}$–H**N**–**C**=C, (N sp^2 planar)	1.339	N1′-C*x* (in **101**, **155**-**157**)
C=**C**–C=O (C,H subst., conjugated)	1.340	C*x*-C11
C=**C**–**C**(=O)(–C^{*}) (conjugated)	1.464	C11-C10
C=C–**C**=**O** (ketones and aldehydes)	1.222	C10-O2

Table 33: Comparison between reference bond lengths [127] and the "enaminone" bond lengths in Table 32.

It can be seen from Tables 32 and 33 that the enaminone functional group is indeed quite unique, as the bond lengths found in this group are not directly comparable to the reference bond lengths given in Table 33. The N1′-C*x* distances in all the model enaminones do compare quite favourably with the reference value in Table 33. However, in the case of the secondary enaminones, this distance is in each case shorter (< 1.33 Å) than expected (1.339 Å). This can be explained by extended conjugation of the N–C bond in these compounds with the carbonyl bond, which is electron-withdrawing. The shortest N1′-C*x* bond in the series is that of the 5-ring analogue. It is important to note that, owing to the electron-donating nature of the alkyl substituents in the tertiary enaminones, the N-C*x* bonds are longer than in the secondary enaminones. It can be seen that the "double" bond C*x*-C11 is in each considerably longer in the enaminones than the reference distance (1.340 Å). In this case, electron-donation from the nitrogen atom in the enaminone lengthens this bond slightly, relative to the given reference value. The C*x*-C11 bond is especially long (1.402 Å) in the 8-ring analogue **157**, and considerably shorter in the 5-ring analogue **155** (1.364 Å). It can therefore be deduced that electronic donation from the ring

nitrogen is least prominent in the enaminone group of **157**, and most so in **155**. The C11–C10 bond is shorter in all the enaminones studied than the reference bond given for the same reason (extensive conjugation). In the series studied, this bond is again the shortest in the 5-ring analogue (1.401 Å). The carbonyl C=O bond is longer in the enaminones than the reference value given for a conjugated carbonyl bond in Table 33. Once again, this is the result of extended conjugation of the carbonyl group within the enaminone, together with the electron-withdrawing effect of intramolecular hydrogen bonding in the case of the secondary enaminones. As expected, the carbonyl bond in this series is the longest (1.254 Å) for enaminone **172**, since the phenyl substituent in **172** draws electron density away from this carbonyl bond. However, the carbonyl bonds in the free N*H* analogues are not considerably shorter than that in **172**, since these carbonyl oxygens are involved in relatively strong intramolecular hydrogen bonding. Also as expected, the carbonyl bond is the shortest (1.235 Å) in the cyanoethyl protected analogue **146**, since no intramolecular hydrogen bonding is possible in this compound. The other three bonds in the proximity of the enaminone group (i.e. the bottom three rows, Table 32) are of expected magnitude and therefore not much affected by the neighbouring enaminone group. It can be seen, however, that the endocyclic N1′-C2′ bond is slightly longer in the *N*-alkylated derivatives **172** and **146**. This observation, together with the lengthening of the N1′-C*x* bonds in **172** and **146**, is a reflection of the slightly greater electron-donating ability of the alkyl groups (in contrast to the hydrogen involved in hydrogen bonding in the secondary enaminones) on the amine nitrogen. The enaminone nitrogens in **172** and **146** are therefore also expected to be slightly more basic than those in the free *N*H derivatives. The intramolecular N1′-O2 close contacts [N1′(donor)···O2 (acceptor)], which arise from hydrogen bonding, clearly decrease with an increase in the ring size of the enaminone containing ring. This is graphically represented in Figure 42(a). As the ring size increases, the enaminone nitrogen is forced progressively closer towards the central ketone oxygen. In the pyrrolidinylidene derivative **155**, geometrical constraints prevent a closer approach (than *ca*. 2.9 Å) between N1′ and O2. This distance decreases as the ring size increases for steric reasons. Figure 42(b) represents graphically the change in “true” intramolecular hydrogen bond length, i.e. the distance between O2 and H1′, with increase in ring size. It can be seen that this distance does not decrease smoothly as observed for the O2-N1′ distance [Figure 42(a)]. Instead, the six-, seven- and eight-membered cyclic analogues contain similar O2-H1′ bond

lengths, which approximate a minimum separation for atoms O2 and H1′. The five-membered analogue **155**, however, contains a considerably longer O2-H1′ bond than the other compounds in the series. The bond angles in the enaminone groups are tabulated below in Table 34.

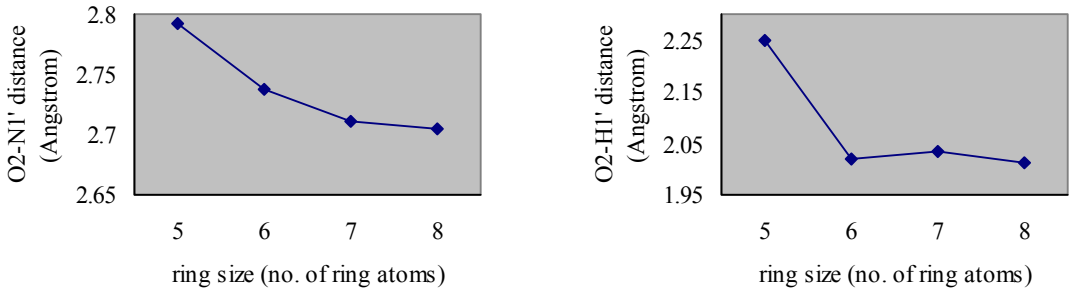

(a) (b)

Figure 42: Variation in intramolecular hydrogen bond length with enaminone ring size.

Bond angle	**172**	**146**	**101**	**155**	**156**	**157**
N1′-C*x*-C11	120.94(16)	121.6(2)	122.76(16)	127.0(3)	121.3(2)	121.39(16)
C*x*-C11-C10	125.50(16)	126.5(2)	124.16(17)	123.8(3)	124.3(2)	123.83(15)
C11-C10-O2	125.79(17)	127.9(2)	125.28(17)	125.0(3)	125.1(2)	124.80(16)
C*y*-C*x*-C11	120.88(16)	120.70(18)	118.99(16)	125.7(3)	120.3(2)	118.91(15)

Table 34: Comparison of the bond angles (in degrees) in the enaminone groups.

It can be seen that the "enone" bond angles, C*x*-C11-C10 and C11-C10-O2, are basically constant (*ca*. 125º) throughout the series. The increase in these sp^2-hybridized bond angles (>120º) serves to keep the electron-rich carbonyl and quinazolinone groups as far away as possible from the enaminone ring. The most obvious differences in the above bond angles are the N1′-C*x*-C11 (i.e. the N1′-C5′-

C11) and C*y*-C*x*-C11 (i.e. C4′-C5′-C11) angles in **155**, which are both considerably larger than the corresponding angles in the rest of the series. Geometrical constraints imposed by the small 5-membered ring in **155** forces these angles to increase slightly above the ideal magnitude (120º). These slightly larger bond angles possibly stabilize the exocyclic double bond in **155** more, relative to the other secondary enaminones, since the ring bonding electrons and the π electrons are kept further apart.

It is clear from the above discussion that the enaminone carbons and nitrogen in the 5-ring analogue **155** is most "shielded" as a whole. The internal enaminone bond lengths are all shorter, and the intramolecular hydrogen bond is considerably longer, in **155** than in the other derivatives (see Table 32). This suggests that the electrons are more localized in the N–C=C–C=O group of **155**.

6.6. Comparison of NMR data

NMR spectroscopy can provide a wealth of information regarding the distribution of electron density in organic compounds. The chemical shift δ (in ppm) of any given hydrogen or carbon atom in an NMR spectrum provides a clear indication of its electronic environment. The ^{1}H and ^{13}C chemical shifts of relevant atoms in, and around, the enaminone groups of selected model vinylogous amides (from Chapter 3) are given in Tables 35 and 36. Note that, in addition to the six model compounds of which the crystal structures were discussed in Sections 6.2 to 6.5, the NMR data of three other enaminones (**143**, **158** and **159**) are also included in this section.

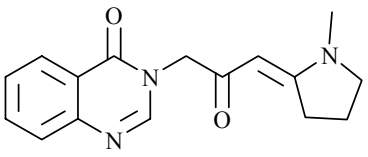

143

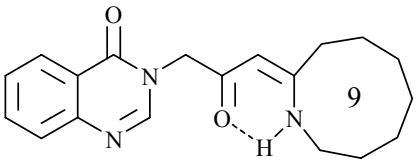

158

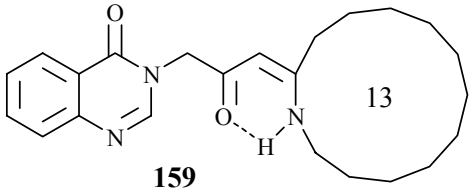

159

A significant difference between the *E*- and the *Z*-enaminones is immediately apparent from Table 35 (selected proton chemical shifts). The ring protons at the α position to the enaminone group (i.e. NCC*H*$_2$) are considerably more deshielded in the *E*-enaminones (**172**, **146**, **143**) than in the *Z*-enaminones. This is as a result of deshielding by the electronegative carbonyl oxygen atom, which is in close proximity to these protons in the *E*-enaminones. The vinyl proton (NC=C*H*) is the most deshielded (δ_H 5.65) in enaminone **172**, owing to the inductive electron-withdrawing effect of the phenyl substituent on this nearby proton in **172**.

As observed before, the 5-ring derivative **155** conforms less than the other analogues in the secondary enaminone series (**155**, **101**, **156-159**). In fact, all three non-equivalent groups of protons on the carbon atoms in the enaminone group of **155** (i.e. the top three rows in Table 35) are more deshielded than in the other compounds of this series (**155**, **101**, **156-159**). This obvious deshielding, particularly of the ring methylene groups (NCC*H*$_2$ and ring NC*H*$_2$), in **155** points again to the "channelling" of electrons from the small piperidylidene ring into the enaminone group. The stronger exocyclic double bond in **155** has the effect of deshielding the NC=C*H* proton more, relative to the other analogues. It is important to note that the ^{1}H NMR chemical shifts of the N*H* protons in this series (i.e. row 4 in Table 35 on the previous page) are dependent on the concentrations of the vinylogous amides in the NMR samples. The more concentrated a sample is the stronger the intermolecular hydrogen bonding interactions might be so that the protons involved in hydrogen bonding will be more deshielded, compared to that in a less concentrated sample. Unfortunately, we did not calculate the exact concentrations of these samples. They were, however, all in the region of 10 mg material dissolved in a relatively standard volume of $CDCl_3$. Comparisons should therefore be made with caution. The exocyclic double bond is presumably stabilized by this effect in the 5-membered ring, and therefore less so in the larger rings. The weaker intramolecular hydrogen bond in **155** is reflected in the considerably lower chemical shift (δ_H 9.83) observed for the N*H* proton in **155**, as compared to the other analogues in this series. In the larger rings, electron density is withdrawn from the enaminone groups by stronger hydrogen bonds. This, in turn,

proton(s) (in italics)	**172**	**146**	**143**	**101**	**155**	**156**	**157**	**158**	**159**
NCC*H*$_2$	3.33	3.17	3.23	2.39	2.63	2.33	2.32	2.34	2.24
ring NC*H*$_2$	3.33	3.43	3.45	3.32	3.57	3.32	3.38	3.41	3.31
NC=C*H*	5.65	5.05	5.07	4.93	5.15	5.03	5.01	4.99	5.02
N*H*	n.a.	n.a.	n.a.	11.11	9.83	10.93	10.96	11.08	10.74

Table 35: Selected proton chemical shifts, δ_H (ppm).

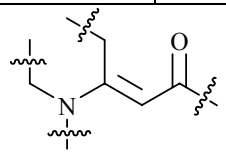

carbon (in italics)	**172**	**146**	**143**	**101**	**155**	**156**	**157**	**158**	**159**
exocyclic N*C*H$_2$/H$_3$	40.2	47.9	33.3	n.a.	n.a.	n.a.	n.a.	n.a.	n.a.
NC*C*H$_2$	28.3	28.0	33.7	28.5	32.6	34.9	32.0	32.4	31.2
ring N*C*H$_2$	52.0	54.4	54.8	41.1	47.8	44.4	41.4	43.8	41.2
NC=*C*H	90.7	89.7	85.6	90.2	86.3	90.9	90.7	90.9	91.8
N*C*=CH	164.8	164.3	168.0	166.5	169.8	172.0	171.2	171.7	169.7
C=O	187.5	186.5	186.4	186.0	187.4	187.3	186.9	186.7	186.7

Table 36: Selected carbon chemical shifts, δ_C (ppm).

could destabilize the exocyclic double bonds. Interestingly, the piperidylidene analogue **101** contains the most deshielded N*H* proton (δ_H 11.11), even though [as seen from the crystal data (Table 32, Section 6.5.)] the intramolecular hydrogen bond in **101** is not the strongest of the series. Furthermore, the N-H bond length in **101** was clearly the longest (weakest) of the series (see Table 32, Section 6.5.). It may therefore be presumed that the NH proton in **101** is most acidic. The enaminone protons in **101** are also generally quite shielded, as indicated particularly by the fact that the CH=C*H* chemical shift in **101** (δ_H 4.93) is the lowest in the entire series.

The ^{13}C NMR shifts shown in Table 36 are generally more constant through the series. It can be seen that the carbon α to enaminone group (NC*C*H_2) is not deshielded in the *E*-enaminones, relative to the *Z*-enaminones, as was observed above for the protons attached to this carbon. The chemical shift of the NC=*C*H carbon in *N*-methylated 5-ring derivative **143**, is the lowest in the series and very similar to that of its 5-ring counterpart **155**. This points again to a higher electron density in the exocyclic double bonds of the 5-membered rings.

The most obvious difference between the *E*- and *Z*-enaminones is the chemical shifts of the ring N*C*H_2 carbons. These are noticeably more deshielded in the *E*-enaminones. Electrons are therefore efficiently "channelled" away from this position into the conjugated enaminone functional group of the *N*-alkylated enaminones (**172**, **146**, **143**). This could explain the relative ease of protonation of the *N*-alkylated enaminones (see Section 3.8.3.), when compared to the free *N*H enaminones. The use of the weaker acid, AcOH, was sufficient to obtain good results during the chemoselective hydrogenation of the *N*-alkylated enaminones over PtO_2. It was found that a stronger acid (HCl) was required to effect the hydrogenation of free N*H* piperidinylidene analogue **101**. Importantly, the NC*H*$_2$ protons are also significantly deshielded in the 5-ring analogue **155** (and more so than in any of the other free N*H* enaminones), which indicates again the higher electron-withdrawing effect of the enaminone group in **155**, compared to the other free N*H* enaminones. It is, in fact, evident from Tables 35 and 36 that **155**, owing to weaker intramolecular hydrogen bonding than in the rest of the *N*H series, has a similar electronic distribution to the *N*-alkylated series. The only obvious difference is that the N-C*x* bond is shorter in **155**

than in the tertiary enaminones (see Section 6.5.). Contrary to what might be expected from the hydrogenation attempts discussed in Section 3.8.2., the C=C double bond in **155** should therefore also be more easily reducible than, e.g. that in **101**. Protonation is thought to be an important step in facilitating the hydrogenation of the exocyclic double bond, by destroying conjugation in the enaminone group. It should be noted that the best result for the selective hydrogenation of **155** was, in fact, observed when AcOH was used as the solvent (see Table 9, Section 3.8.2.), similar to the case for the *N*-alkylated enaminones. However, some evidence of over-reduction was unfortunately observed, and the desired reaction was extremely slow. Importantly, the 5-membered cyclic analogues **155**, **143** and **147** were, in all hydrogenation attempts, either resistant to reduction or over-reduced (when harsher conditions or extended reaction times were applied).

6.7. Conclusion and future work

Organic molecules often react as a result of internal strain and reactions which lead to total an increase in internal strain energy are not favoured processes. High strain energy is generally the result of electron-electron repulsion. The total strain energy in a molecule can be conveniently divided into the following components: bond-length strain, bond-angle strain, torsional strain, and nonbonded repulsion [177]. The difference in the stability and reactivity of exocyclic double bonds in 5- and 6-membered rings might be explained by using this simple principle. Torsional strain results from the non-ideal arrangement of vicinal bonds, e.g. in the eclipsed conformation of ethane. As part of his ongoing study on the difference in the behaviour of exocyclic double bonds in 5- and 6-membered ring, Brown and co-worker Ichikawa determined in 1957 that cyclohexanone is reduced by $NaBH_4$ 23 times faster than cyclopentanone [177]. This can be explained by the difference in the relative torsional strain in the two systems [177]. In a five-membered ring, changing the sp^2 hybridization of a ring atom to sp^3 results in an increase in torsional strain owing to an increase in the number of eclipsed interactions in the saturated five-membered ring. The opposite is true for six-membered rings, in which this change results in a completely staggered (chair) arrangement which reduces torsional strain. Similar reasoning might be applied to the observation that a five-membered ring (containing an exocyclic double bond) is less

likely than an analogous six-membered ring to undergo an isomerization or an elimination reaction which results in an endocyclic double bond. An endocyclic double bond might increase torsional and bond length strain in the smaller five-membered ring, whereas in the six-membered ring such an arrangement might have the opposite effect.

We have shown in this section that the double bond exocyclic to a five-membered enaminone-containing ring is shorter (and therefore stronger) than the double bond in the corresponding six-membered analogue. The electron density is also more concentrated in the conjugated 5-ring enaminone group (which results in the general shortening of C-C and C-N bond lengths in this group) than in the corresponding 6-ring enaminone group. The smaller and electron-poorer five-membered ring therefore in effect seems to be capable of stabilizing the exocyclic double bond more, relative to the situation in the analogous six-membered ring. This might explain the observation that the exocyclic double bond in the 5-membered cyclic enaminone was generally less sensitive to reducing agents than that of the 6-membered analogues (see Section 3.8).

We have also shown that intramolecular hydrogen bonding in the secondary cyclic enaminone series drains electron density away from the enaminone group. In this way, electron delocalization in the secondary enaminone group is further enhanced and the group is stabilized more relative to the situation in the tertiary enaminones, which cannot be stabilized further in this way. Interestingly, this stabilizing effect was most pronounced in the six-membered cyclic secondary enaminone **101**, which is thought to reduce the basicity of the enaminone carbon α to the carbonyl group [i.e. N–C=C–**C**–C(O)] most. A stronger acid (HCl) was therefore required to destroy conjugation in **101**, compared to that used (AcOH) for the *N*-alkylated enaminones. A reduced yield of the desired synthetic alkaloid [(±)-**14**] was therefore obtained in the hydrogenation reaction of **101**, since the reaction required harsher conditions and was consequently less selective than for the *N*-alkylated enaminones.

It might be predicted that, owing to a probable reduction in torsional strain during the conversion of a sp^2 ring carbon to a sp^3 carbon during the hydrogenation of the larger

(> 6-membered ring) secondary enaminones in this series, these compounds might also be more easily hydrogenated than the five-membered ring analogues. Unfortunately, owing to time constraints, these hydrogenation reactions were not conducted. An interesting future project might be to conduct a kinetic study of the hydrogenation reactions in this series. Also, as mentioned before, the antimalarial activity of febrifugine analogues containing alkaloidal rings larger than the piperidine ring have not been determined. Furthermore, an extensive comparison of the IR and UV spectroscopic characteristics in this series of vinylogous amides needs to be conducted. Owing to the loss of conjugation in the enaminone functional group upon protonation, the UV spectra of these compounds change significantly upon protonation [178]. The pK_a-values of the series can therefore be determined and compared. Presumably, the lower the pK_a-value of the enaminone group, the more easily reducible the enaminone C=C bond might be. Future work also includes the possibility of performing molecular mechanics and quantum chemical calculations to quantify both the structural and the electronic effects in the systems. Finally, the crystal structure of the nine-membered cyclic analogue **158** was not yet determined at the time of this thesis write-up (and, unfortunately, the thirteen-membered cyclic analogue **159** in the series was isolated as a liquid and could not yet be induced to crystallize). During several attempts, a suitable single crystal of the nine-membered cyclic analogue **158** could not yet be found. It is predicted that the structure of **158** might be interesting, as the melting point of **158** (172-174 ºC) is considerably higher than that of the 8-membered analogue **157** (149-150 ºC) and a significant difference in the solid-state structures of these two compounds might therefore be anticipated.